10

Atomic Manipulation on an Insulator Surface

Sabine Hirth, Frank Ostendorf, and Michael Reichling

Abstract. The manipulation of atomic and molecular species on metal surfaces with the scanning tunneling microscope (STM) operated at low temperature is a well established method for bottom-up nanofabrication [G. Meyer et al., Single Mol. **1**, 79 (2000); N. Lorente, R. Rurali, H. Tang, J. Phys. Condens. Matter **17**, S1049 (2005)], but is limited in its understanding and applications by restrictions inherent to the STM technique. These limitations can be overcome by using a dynamic scanning force microscope (SFM) for atomic manipulation that offers three major advantages compared to STM. First, the force microscope allows a quantification of the forces applied during the manipulation process (see Chap. 9), second, it facilitates manipulation at room temperature (see Chaps. 8 and 11) and, third, the technique allows manipulation on electrically insulating surfaces. However, examples for force controlled manipulation of atomic size species on an insulator surface are still scarce regarding experimental evidence [S. Hirth, F. Ostendorf, M. Reichling, Nanotechnology **17**, S148 (2006); R. Nishi et al., Nanotechnology **17**, S142 (2006)] as well as theoretical explanation [T. Trevethan et al., Phys. Rev. Lett. **98**, 028101 (2007); T. Trevethan et al., Phys. Rev. B **76**, 085414 (2007)]. Here we demonstrate the force controlled manipulation of water related defects on a $CaF_2(111)$ surface by a raster scanning motion of the tip over a specific surface region. Manipulation is facilitated by repulsive forces exerted by approaching the tip very closely to the defects. We focus mainly on the presentation of manipulation results and discuss the circumstances that allow a control of the manipulation process. The $CaF_2(111)$ surface is specifically well suited for such studies as this surface has been very well characterized by NC-AFM in previous studies [M. Reichling, C. Barth, Phys. Rev. Lett. **83**, 768 (1999); C. Barth, M. Reichling, Surf. Sci. **470**, L99 (2000); F.J. Giessibl, M. Reichling, Nanotechnology **16**, S118 (2005); R. Hoffmann et al., J. Am. Chem. Soc. **127**, 17863 (2005)] and contrast formation is understood on a quantitative level [A.S. Foster et al., Phys. Rev. Lett. **86**, 2373 (2001); C. Barth et al., J. Phys. Condens. Matter **13**, 2061 (2001); A.S. Foster et al., Phys. Rev. B **66**, 235417 (2002)]. Furthermore, the geometric and electronic structures of this surface is well understood from a variety of theoretical simulations [A.V. Puchina et al., Solid State Commun. **106**, 285 (1998); V.E. Puchin et al., J. Phys. Condens. Matter **13**, 2081 (2001); Y. Ma, M. Rohlfing, Phys. Rev. B **75**, 205114 (2007); Y. Ma, M. Rohlfing,

S. Morita et al. (eds.), *Noncontact Atomic Force Microscopy*,
NanoScience and Technology,
DOI: 10.1007/978-3-642-01495-6_10,

Phys. Rev. B **77**, 115118 (2008)]. Therefore, it can be expected that the experimental evidence of force controlled manipulation presented here will finally be fully explained by further theoretical modeling.

10.1 Introduction

The manipulation of atomic and molecular species on metal surfaces with the scanning tunneling microscope (STM) operated at low temperature is a well established method for bottom-up nanofabrication [1, 2], but is limited in its understanding and applications by restrictions inherent to the STM technique. These limitations can be overcome by using a dynamic scanning force microscope (SFM) for atomic manipulation that offers three major advantages compared to STM. First, the force microscope allows a quantification of the forces applied during the manipulation process (see Chap. 9), second, it facilitates manipulation at room temperature (see Chaps. 8 and 11) and, third, the technique allows manipulation on electrically insulating surfaces. However, examples for force controlled manipulation of atomic size species on an insulator surface are still scarce regarding experimental evidence [3, 4] as well as theoretical explanation [5, 6]. Here we demonstrate the force controlled manipulation of water-related defects on a $CaF_2(111)$ surface by a raster scanning motion of the tip over a specific surface region. Manipulation is facilitated by repulsive forces exerted by approaching the tip very closely to the defects. We focus mainly on the presentation of manipulation results and discuss the circumstances that allow a control of the manipulation process. The $CaF_2(111)$ surface is specifically well suited for such studies as this surface has been very well characterized by NC-AFM in previous studies [7–10] and contrast formation is understood on a quantitative level [11–13]. Furthermore, the geometric and electronic structures of this surface is well understood from a variety of theoretical simulations [14–17]. Therefore, it can be expected that the experimental evidence of force controlled manipulation presented here will finally be fully explained by further theoretical modeling.

10.2 Basic Principles

10.2.1 Experimental Procedures

Manipulation experiments are performed in an ultra-high vacuum (UHV) chamber operated at a base pressure below 1.3×10^{-8} Pa. The system is equipped with a commercial dynamic scanning force microscope UHV 350 from RHK (Troy, Michigan, USA), providing highest resolution and stability during imaging and manipulation. Procedures of sample preparation and atomic resolution imaging are similar to those used in previous studies of the $CaF_2(111)$ surface [11, 12]. The crystal is kept at room temperature during all experiments. For imaging and manipulation, commercial, uncoated,

conductive silicon cantilevers with resonance frequencies of 60–70 kHz and spring constants of a few Nm^{-1} are used. Q values are above 80,000 in the UHV. The cantilever oscillation amplitude is kept constant at a level of 18–25 nm. All tips can be assumed to be covered with a native silicon oxide layer when purchased. Tips are used without further treatment like sputtering or flashing; only a bakeout at 120°C overnight is performed to remove volatile surface contaminants. For best imaging contrast, the contact potential is minimized by adjusting the sample bias to a voltage of typically +0.6 V. The contact potential is determined via Kelvin probe force spectroscopy ($U_{\mathrm{mod}} = 100\,\mathrm{mV}$) [18, 19]. During imaging, the cantilever resonance frequency detuning is typically −20 Hz. The topography feedback is set to a very slow time constants (1.5 s), facilitating imaging in the quasi constant height mode [20]. Images are taken at a scan speed of 300 ms per line and, although the feedback is slow compared to the line acquisition time, we can readily pick up topography information under these circumstances. When manipulating defects, we follow a protocol based on regular line-by-line scanning of the surface as used for imaging. For manipulating defects present in a certain area, the respective region is raster-scanned, with the detuning increased to typically 35 Hz. Successful manipulation appears in the resulting high contrast images as a chain-like manipulation path with an overall direction that is not related to the scanning direction in a simple way. When the desired position is achieved, the tip is retracted from the surface by reducing the detuning to 20 Hz or even lower values. Under the latter conditions, the defect is not manipulated but can be imaged without severe perturbation. The $CaF_2(111)$ sample with a size of $2 \times 10 \times 3\,\mathrm{mm}^3$ (Korth Kristalle GmbH) is prepared by cleavage of a longer rod in UHV at base pressure and room temperature inside the microscope. A successful preparation yields large atomically flat terraces divided by steps having a height of integer multiples of the F–Ca–F triple layer height (315 pm). Immediately after cleavage, terraces are found to be absolutely clean and contamination at step edges that could result from trapping of diffusing molecules cannot be detected even in traces. In images shown below, the direction of slow scanning is indicated by the solid arrow (filled triangle) in the upper left or right corner. Fast scanning is performed perpendicular to this direction in alternating lines from left to right (⇒) and right to left (⇐).

10.2.2 Surface Characterization

The $CaF_2(111)$ surface is a prototype insulating surface that is well understood in its NC-AFM atomic contrast formation. The surface consists of stacked triple layers with a height of 315 pm. Fluoride forms the first and third layer and the cubic sites are filled by calcium ions that are missing in every second of the gap rows. It has been shown that contrast formation strongly depends on tip polarity as demonstrated in Fig. 10.1, combining

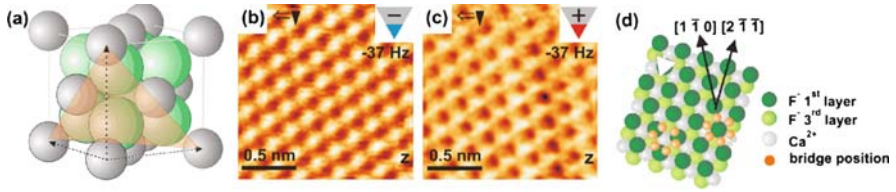

Fig. 10.1. Schematic representation and NC-AFM scanning results for the $CaF_2(111)$ surface. (**a**) unit cell of CaF_2; small spheres represent calcium and large spheres the fluoride lattice. The (111) plane is represented by the shaded triangle. Images (**b**) and (**c**) demonstrate the two basic contrast patterns found in NC-AFM imaging for negatively and positively terminated nano tips, respectively. Pane (**d**) shows a model of the (111) surface with an assignment of surface directions as present in images (**b**) and (**c**). The small spheres indicate the positions bridging either fluorine or calcium sites. The orientation of the hexagon defined by the bridging sites is the same in both cases (From [3])

structural models of the crystal and the (111) surface with NC-AFM imaging results [11].

A negatively terminated tip images calcium ions as bright circular features, but the calcium sub-lattice does not provide unambiguous information about surface directions. When imaging with a positively charged tip, a triangular contrast is observed that is formed by a superposition of interactions between fluoride in the first and third row of a triple layer [12]. The corners of the triangle are determined by the low lying fluoride ions as depicted (white triangle) in panel (d). This ability of the NC-AFM to image both fluorine sub-lattices allows an unambiguous identification of all directions in the surface plane. NC-AFM images demonstrating results for both tip terminations shown in panels (b) and (c) have been taken on the crystal used for the manipulation experiments. From these images we can deduce the crystal orientation that is the same for all other images shown later. Therefore, we have an absolute coordinate system for the description of the different manipulation pathways on the surface. As will be shown later, the analysis of manipulation images reveals a point of maximum interaction at bridge positions between apparent protrusions. These positions are marked in red in panel (d) and can either represent positions bridging calcium or fluorine ions. A comparison of the two bridge positions observed for tips of different polarity shows that these positions are shifted by a small distance, but the angular orientation of the hexagon of bridge positions is the same in both cases. Therefore, the two bridge positions can be seen as equivalent for the following discussion. A careful analysis of the lattice contrast performed for many images reveals that in most cases imaging is performed with a negatively terminated tip. Hence, in the vast majority of images, a disk-like contrast is observed [12]. Furthermore, great care was taken to avoid and detect atomic tip changes that would strongly change lattice and defect contrast formation. Manipulation experiments involving strong

tip–surface interaction could in a reproducible manner only be performed with exceptionally stable, negatively terminated tips.

10.3 Experimental Results

10.3.1 Defect Preparation and Contrast Formation

It is well known from NC-AFM imaging experiments on CaF_2 crystals cleaved in air and on surfaces dosed with gases after vacuum cleavage that the (111) surface of CaF_2 is readily degraded by water and oxygen [7, 21]. This leads to the formation of randomly distributed nanometer-sized features protruding from the surface by typically less than 100 pm, that is, much less than the triple layer step height. When exposing the surface to small amounts of water, one observes the evolution of two types of atomic scale defects, namely stationary defects firmly pinned to a lattice site and mobile defects that may be moved from one site to another by the action of the scanning tip. The mobile species is found only after few days of measurement in the presence of a large number of stationary defects. We interpret this in a model proposing that water reacts with different types of vacancies on the surface and one type of reactive center is saturated after a while, and afterwards water reacts with the less abundant second type of vacancy. Based on preliminary theoretical studies of water molecules interacting with surface vacancy defects on $CaF_2(111)$, we associate the stationary defect with a hydroxyl group embedded into the surface at the site of a former neutral surface F center (F^0), while the mobile defect is associated with a water molecule attached to a charged surface F center (F^-). [22] An easy way of surface preparation for low dosages is simply exposing the surface to the residual gas of the vacuum system that mainly contains water. Phenomena observed in such an experiment do not differ qualitatively from those observed for deliberate water dosage but the formation of surface defects is very slow, facilitating a detailed observation of the development. The series of images taken over a total time of 144 h shown in Fig. 10.2 provides an overview of the degradation of $CaF_2(111)$ under UHV conditions in a frame size of 300 by 300 nm. Defects emerging with time are marked by circles for better visibility.

Occasionally, very few clusters cover the surface directly after cleavage (Fig. 10.2a) and as frames (b)–(d) show, contamination is continuously built up. The last two frames are assembled from four smaller panes as scanning larger frames became increasingly difficult with an increasing number of contaminants present. The last image of the series exhibits chain-like features that are indications for manipulation events. The manipulation paths extend over several tenth of nanometers and we note the preferential direction of manipulation in independently scanned panes. All manipulation paths are roughly parallel and deviations are caused by scanner piezo creep as the frames were taken consecutively at different positions without giving the piezo time to equilibrate after the previous scanning motion. Figure 10.3. is a study of contrast

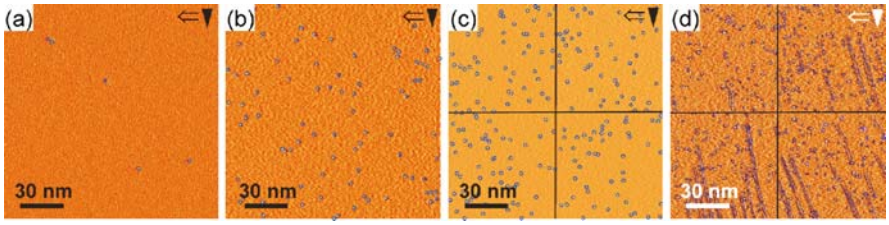

Fig. 10.2. Degradation of a $300 \times 300\,\mathrm{nm}^2$ area on an atomically flat $CaF_2(111)$ surface observed in UHV as a function of time. Circles mark contaminants on the surface, a few resulting from the preparation but most of them developing under the influence of the residual gas. The black lines in frames (**c**) and (**d**) mark the boundaries of the four smaller images that were assembled to form the larger frame. Image (**a**) shows the surface directly after cleavage. Frame (**b**) shows an increased density of impurities after three days. In frame (**c**), the contamination level is further increased after the fifth day. Frame (**d**) shows a high density of impurities as observed on the ninth day after cleavage. The quasi-parallel lines indicate the manipulation of certain defects over distances of several ten nanometers (From [3])

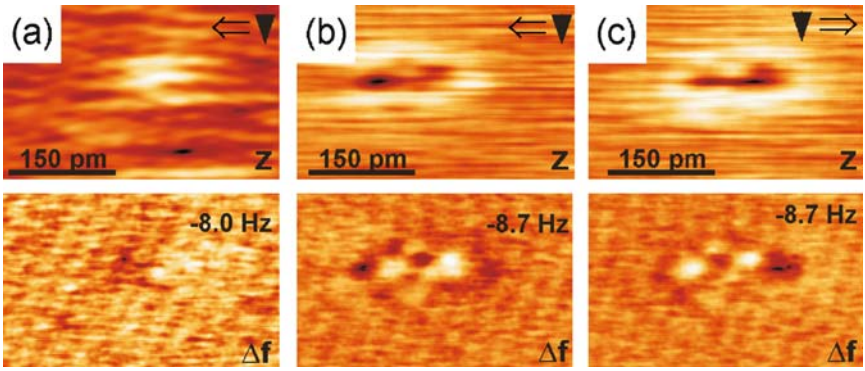

Fig. 10.3. Contrast formation studied on a stationary atomic size defect. Shown are simultaneously recorded topography and detuning images. Frames (**b**) and (**c**) have been recorded at an increased average detuning compared to frame (**a**). The increase of 0.7 Hz in detuning results not only in an increased contrast but also a contrast inversion. The apparent elongation of the defect and the characteristic pattern involving dark and bright contrast points to a repulsive interaction of the foremost tip ions with the defect (From [3])

formation for imaging a stationary defect at different tip–surface distance. When scanned with a relatively large tip–surface distance, defects appear as protrusions; however, they change their appearance to that of an indentation with a protruding rim when approaching the surface and scanning in a detuning range that resolves individual lattice sites. This predominant contrast is shown in frames (b) and (c) representing the same defect imaged in forward and backward scanning direction, respectively.

The apparent depth of defects ranges from 10 to 25 pm but as the topography feedback is quite slow, this number is not of great significance. We anticipate that contrast inversion is the result of a complex interaction of the negatively terminated tip with a hydroxyl group. At large tip–surface distance, the partially positive protruding hydrogen causes an enhanced attractive interaction with the tip and the defect appears as a protrusion. When decreasing the tip–surface distance, the interaction with the hydrogen may become repulsive and additionally there is a repulsive interaction with the oxygen that might be exposed as the hydrogen is pushed aside. This scenario is in line with a general model that has been developed for contrast inversion at protruding surface defects [23].

10.3.2 Manipulation of Mobile Defects

Defects found to be mobile on $CaF_2(111)$ can be moved by the interaction with the tip, in a fashion demonstrated in Fig. 10.4. Frames (a)–(g) are consecutively recorded images that have either been taken in the imaging mode at a detuning of −20 Hz or in the manipulation mode at a detuning of −35 Hz. In this experiment, apparently a group of defects is manipulated on the scale of several nanometers first upwards (frames (a)–(c)) and then downwards (frames (d) and (e)). To explore the dependence of the manipulation direction from

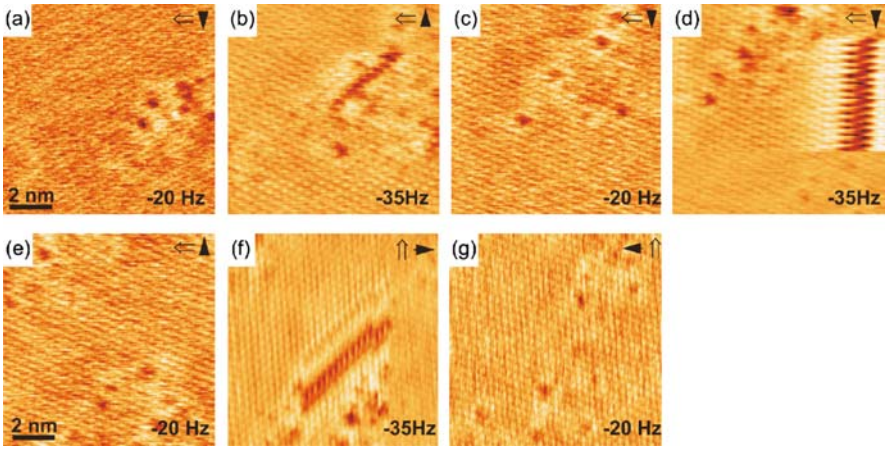

Fig. 10.4. Manipulation of a group of defects on the $CaF_2(111)$ surface. Frames (**a**), (**c**), (**e**), and (**g**) were taken in the imaging mode with an average detuning of −20 Hz. Frames (**b**), (**d**), and (**f**) show manipulation performed with an average detuning of −35 Hz. The chain structure is caused by the repeated imaging of the same defect in the course of manipulation. The direction of manipulation in frames (**b**) and (**f**) is identical despite the interchange of slow and fast scanning direction. The manipulation paths of images (**b**) and (**d**) recorded with opposite slow scanning direction enclose and angle of 120° (From [3])

the scanning direction, in a last manipulation step the fast and slow scanning directions are interchanged (frames (f) and (g)). As the group is initially close to one side of the imaging frame, defects are partially dispersed and the final pattern of the group of defects is different from the initial one. The strong interaction between tip and defect during scanning in the manipulation mode is apparent in the form of strong contrast features forming lines along the main manipulation direction. In none of the images, the direction of manipulation is related to the scanning direction in a trivial way. It is assumed that manipulation occurs via a hopping mechanism where consecutive positions are reached by the interaction of the defect with the tip and neighboring ions. By the action of the tip, defects are first weakly displaced in a potential trough associated with one ionic site. Hopping motion over trough wells results in an abrupt change of the contrast.

In this context it is interesting to investigate the manipulation pathways in frames (b), (d), and (f) of Fig. 10.4. These pathways appear as lines enclosing an angle of 120° with each other. This strongly indicates that defects move along specific crystallographic directions on the surface. Another interesting feature is the width of the manipulation paths. In frame (b), a chain of one minimum per position is observed while image (d) indicates at least two minima along the line, sometimes even three pronounced minima. Although the direction of manipulation in frames (b) and (f) is the same, the appearance of the pathway is different. The minimum along the line appears elongated, indicating a longer manipulation path along the fast scanning direction. We anticipate that this elongation is an effect of movement within the potential trough. Remarkably, mostly more than one defect is manipulated and we assume that this is due to the fact that manipulation is not only performed by the tip terminating cluster providing the atomically resolved image, but also by the force field of larger parts of the tip apex.

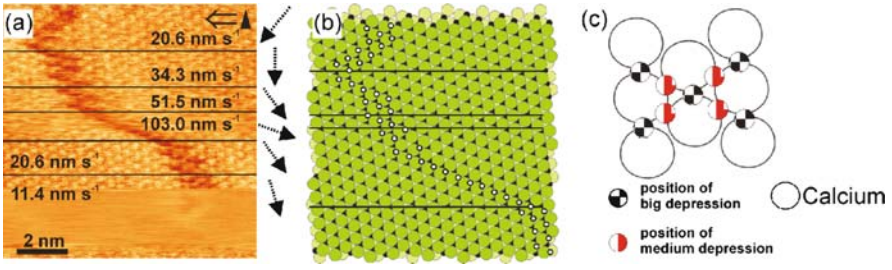

Fig. 10.5. Velocity dependence of the manipulation path. (**a**) A topography image recorded in the manipulation mode where the scanning speed is changed in a systematic manner. The image is taken at an average detuning of −35 Hz. The *dotted arrows* denote the preferential direction of movement as deduced from the resulting image. (**b**) The surface with indicators of preferential sites during manipulation. (**c**) Detailed schematic representation of bridging sites possibly attained during manipulation (From [3])

10.3.3 Velocity Dependence of Manipulation

The direction of manipulation can be influenced by a variation of the scanning speed as is illustrated in Fig. 10.5. The manipulation path is shown in pane (a), while in pane (b) a series of positions is marked that are presumably occupied during defect movement, and pane (c) describes two different bridging positions that apparently play a role for the manipulation process. At slow scanning speed, the path of the defects appears to be broader than that for fast scanning, and hopping occurs more often in the direction of the slow scanning direction for both, forward and backward scanning motion. With increased scanning speed, the visible manipulation path becomes more narrow but the manipulation is more directional. By a careful selection of scanning speed, virtually any manipulation direction is accessible as is indicated by the dotted arrows next to pane (a). Therefore, the method does not only allow the demonstration of simple manipulation events but could principally also be used to perform more sophisticated manoeuvres. The sketch shown in Fig. 10.5c demonstrates that the defect is confined in a rhomb defined by four calcium ions marked by segmented small circles. The quartered circles in image (c) mark positions that are deeper than those marked with half-filled circles. This indicates that the interaction with the tip at these positions is weaker or the defect is more mobile. Most probably, preferred hopping directions are along the threefold hollow sites between the calcium ions and the nearest bridging positions to a point of large depression.

With an orientation of the substrate as indicated in Fig. 10.5(c), the hopping to neighboring bridge sites is not equal for all directions. Because of the angle between a symmetry axis of the substrate and the fast scanning direction, it is likely that the potential energy path along those lines is not the same, effectively leading to different probabilities for a hopping event. When the scanning is very slow, the interaction time of tip and defect might be sufficient to trigger the jump to the left although that might not be the kinetically most favored route. Therefore, we expect that in more elaborate studies it will be possible to define the direction of manipulation by a proper choice of the scanning direction with respect to the crystallographic directions.

10.4 Conclusions

The experimental evidence presented here clearly demonstrates the possibility of force controlled manipulation of a water related defect on the $CaF_2(111)$ surface. While a detailed understanding of the manipulation mechanism requires many further efforts, here we outline a few important points providing a preliminary understanding of the process. The key assumption is that the main interaction resulting in the manipulation is repulsive and manipulation is facilitated by a series of hopping events during scanning in both directions. When the tip is relatively far away from the defect, repulsion causes a local relaxation in form of an evasion of the defect inside a potential trough associated with a neighboring lattice ion. Upon approach, the repulsive force

becomes increasingly stronger and when exceeding a certain limit, hopping motion occurs from one potential trough into another. However, the sequential formation of stationary and mobile defects strongly indicates that the manipulated defect is not simply a molecule but a complex formed by a molecule and a surface vacancy defect. Indeed, preliminary theoretical calculations indicate that water dissociates and forms hydroxide as a stationary defect when interacting with surface F^0 centers. On the other hand, a water molecule can bind to an F^- center and form a mobile defect. Mobility is created by lowering the diffusion barrier for the water/F^- complex in the force field of the scanning tip [22]. In the framework of this model, manipulation is a rather complex process involving surface relaxation and the motion of the adsorbed species together with a vacancy defect. Pinning the water molecule to the vacancy prevents diffusion at room temperature if the tip is absent, while manipulation is facilitated by thermal diffusion over a reduced barrier in the presence of the tip.

Acknowledgments

The authors are most grateful to A. Foster for many contributions to the interpretation of experimental results and sharing his simulation results with the authors and to R. Nishi, Y. Sugimoto, A. Shluger, and S. Gritschneder for stimulating discussions.

References

1. G. Meyer et al., Single Mol. **1**, 79 (2000)
2. N. Lorente, R. Rurali, H. Tang, J. Phys. Cond. Matter **17**, S1049 (2005)
3. S. Hirth, F. Ostendorf, M. Reichling, Nanotechnology **17**, S148 (2006)
4. R. Nishi et al., Nanotechnology **17**, S142 (2006)
5. T. Trevethan et al., Phys. Rev. Lett. **98**, 028101 (2007)
6. T. Trevethan et al., Phys. Rev. B **76**, 085414 (2007)
7. M. Reichling, C. Barth, Phys. Rev. Lett. **83**, 768 (1999)
8. C. Barth, M. Reichling, Surf. Sci. **470**, L99 (2000)
9. F.J. Giessibl, M. Reichling, Nanotechnology **16**, S118 (2005)
10. R. Hoffmann et al., J. Am. Chem. Soc. **127**, 17863 (2005)
11. A.S. Foster et al., Phys. Rev. Lett. **86**, 2373 (2001)
12. C. Barth et al., J. Phys. Condens. Matter **13**, 2061 (2001)
13. A.S. Foster et al., Phys. Rev. B **66**, 235417 (2002)
14. A.V. Puchina et al., Solid State Commun. **106**, 285 (1998)
15. V.E. Puchin et al., J. Phys. Condens. Matter **13**, 2081 (2001)
16. Y. Ma, M. Rohlfing, Phys. Rev. B **75**, 205114 (2007)
17. Y. Ma, M. Rohlfing, Phys. Rev. B **77**, 115118 (2008)
18. M. Nonnenmacher, M.P. O'Boyle, H.K. Wickramasinghe, Appl. Phys. Lett. **58**, 2921 (1991)
19. U. Zerweck et al., Phys. Rev. B **71**, 125424 (2005)
20. S. Gritschneder et al., Nanotechnology **16**, S41 (2005)
21. M. Reichling et al., Surf. Sci. **439**, 181 (1999)
22. A. Foster, private communication
23. P. Rahe et al., Phys. Rev. B **77**, 195410 (2008)